Chapter 5

Interval-velocity estimation: field-data example

5.1 Data description and preprocessing

Amoco Production Company and Seismograph Service Limited provided a data set from the North Sea to test the velocity-estimation method of this thesis. The survey line was collected over a salt dome in the dominant-dip direction of the surrounding sediments so an assumption of 2-D geology is reasonable. Figure 5.1 shows a single shot profile from the data set. The recording cable was approximately 3 km long with a near offset of 100 meters; there were 180 channels recorded with a group interval 16.66 m. The shot interval was 25 m.

For my purposes, the deepest event of interest is the bottom-of-salt reflection that arrives around or before 2 seconds two-way traveltime; so I retained only the inner 120 offsets from each shot profile for further processing. The data beyond 2 km offset arriving before 2 seconds is dominated by refracted arrivals that propagate only in the near surface. Figure 5.2 shows the near-offset section from the data. The data from the first 12 km of the line and near the top of the salt dome are masked by strong water-column reverberations; elsewhere, sea-floor and pegleg multiples are evident. These events detract from stacked images and also make velocity analysis more difficult, so I applied gapped deconvolution to attenuate them as much as possible. Figure 5.3 shows the near-offset section after gapped decon; most of the "ringy" appearance of the first part of the line and many of the multiples are suppressed. Refer back to Figure 1.1 to see a CMP-stacked section of the

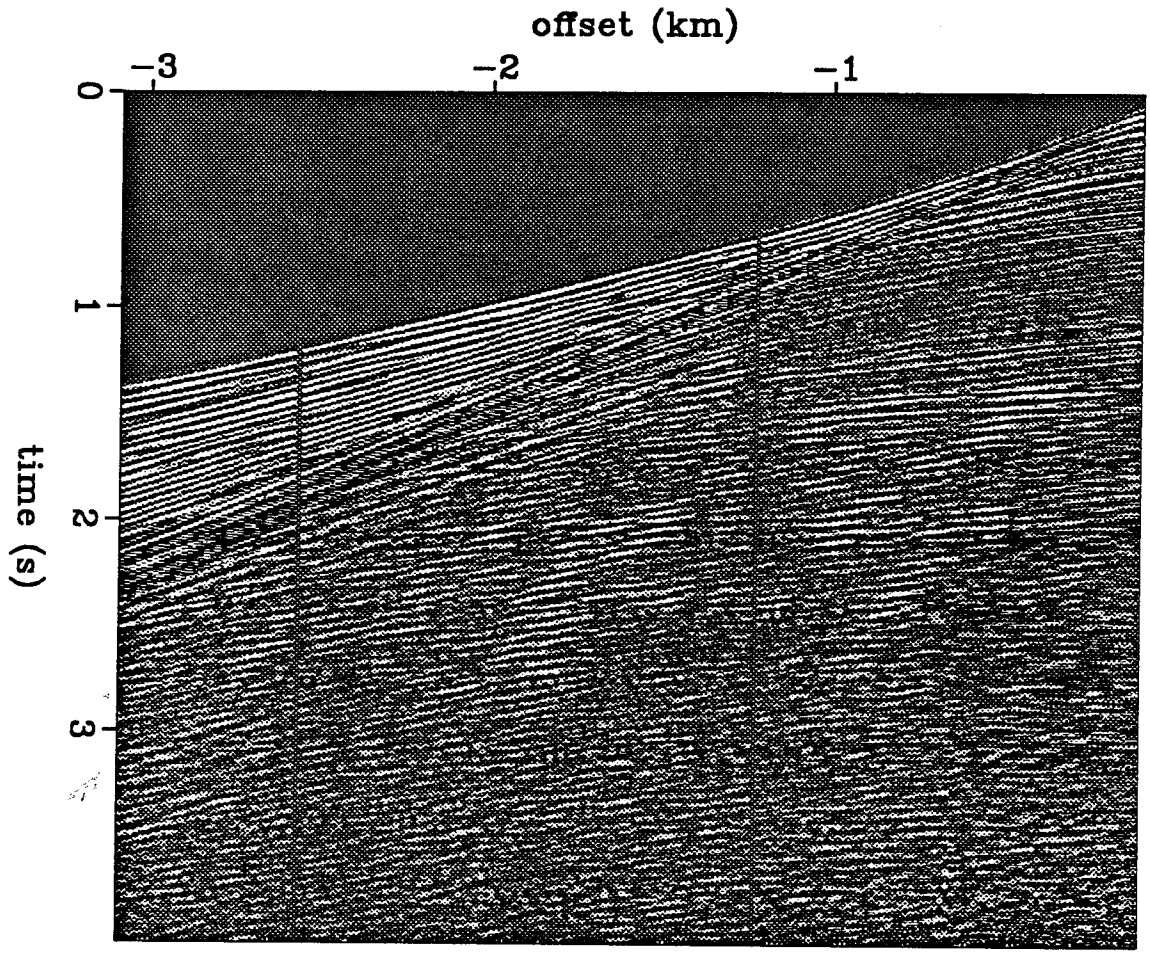

FIG. 5.1. Shot profile from the North Sea data set. The data have been gained by $t^{1.5}$. Note the strong refracted arrivals, particularly past -2 km offset.

data set. The primary exploration target in this data set is the bottom-of-salt reflector. The reflected waves from the bottom of salt are strongly distorted by lateral velocity contrasts between the overlying dipping beds and the salt dome, so depth migration is needed to position the image of the bottom of salt in depth.

5.2 Iterative depth migration and velocity estimation

The velocity-analysis algorithm of Chapter 4 begins with an initial prestack depth migration of the data. Using stacking velocities and a simple geological model, I constructed the interval-velocity model shown in Figure 5.4. I did not try to make the initial model

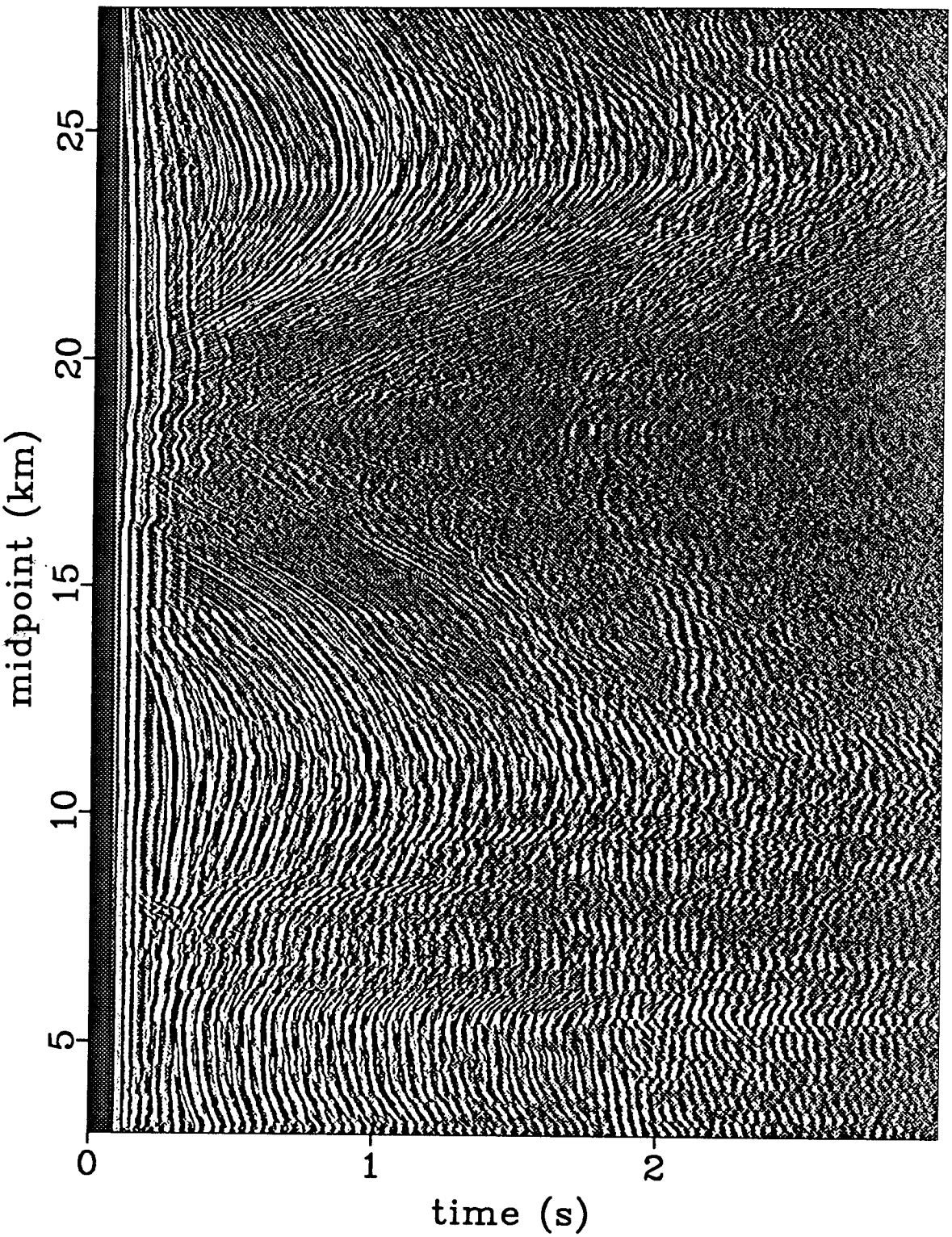

FIG. 5.2. Near-offset section from the data set. Note the strong water-column reverberations around midpoint 12 km. Also note the water-bottom multiples near the top of the salt dome and pegleg multiples on the bottom-of-salt reflector at 24 km, 2 sec.

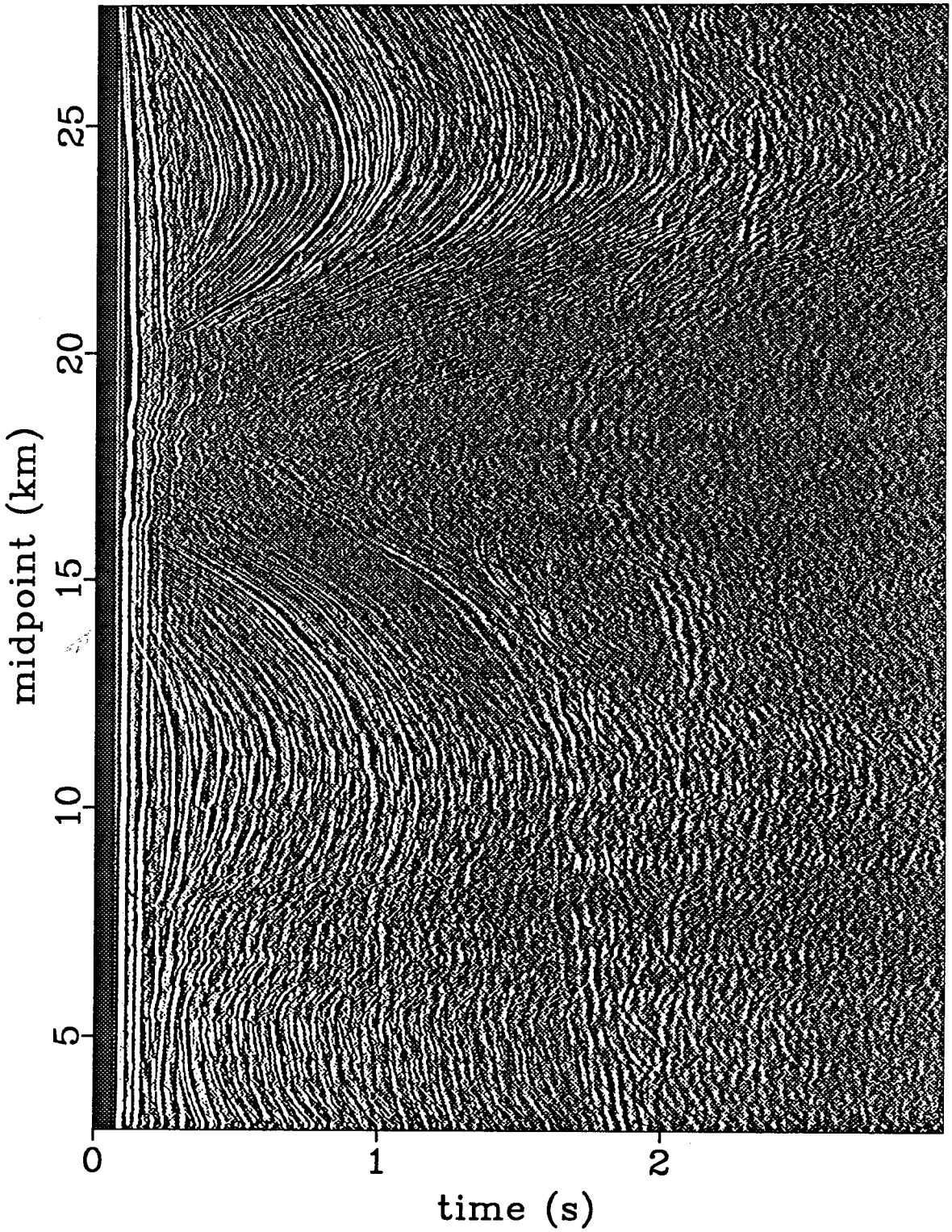

FIG. 5.3. Near-offset section after gapped decon. Most of the water-column reverberations and pegleg multiples are attenuated. Some of the water-bottom multiples remain.

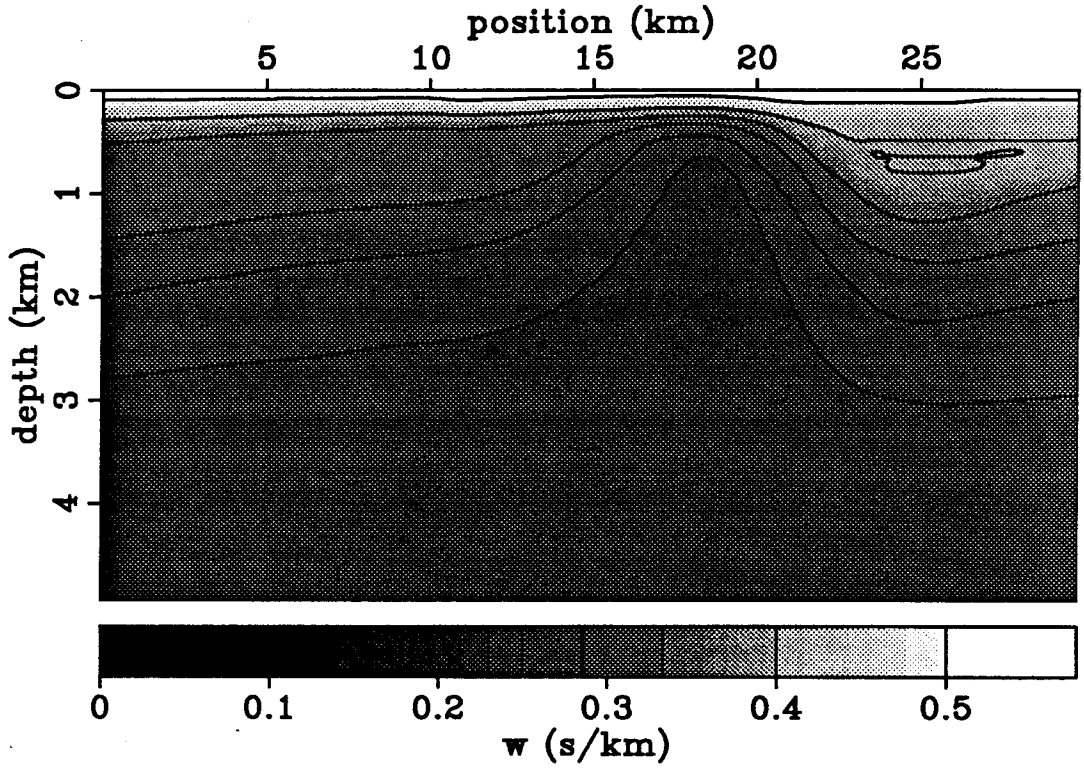

FIG. 5.4. Initial model used for constant-offset prestack depth migration.

particularly accurate since the velocity-estimation procedure should uncover and correct any errors. However, I did try to account for some of the lateral velocity variation induced by the salt dome and the presence of faster rocks on the flanks of the salt dome. Figure 5.5 shows the stacked section after prestack depth migration using the initial interval-slowness model. The high velocities (or low slownesses) in the middle of the initial model cause the image of the bottom-of-salt reflector to be pushed down to nearly the same level as the bottom of salt away from the salt dome, to about 4 km in depth.

Figure 5.6 shows several post-migration CMP gathers. Varying amounts of residual moveout are evident. The shallow reflectors, down to about 2.5 km in depth are curved downward from near offsets to far offsets, indicating the "average" slowness above these reflectors is too low (velocity is too high). The bottom-of-salt reflector in the lowest three panels (3.8 km to 4.0 km) is flat or curving slightly downwards as offset increases indicating correct or slightly low average slowness. In the fourth panel the bottom-of-salt reflector (4.1 km) curves upward as offset increases indicating that the average slowness is too high (velocity is too low).

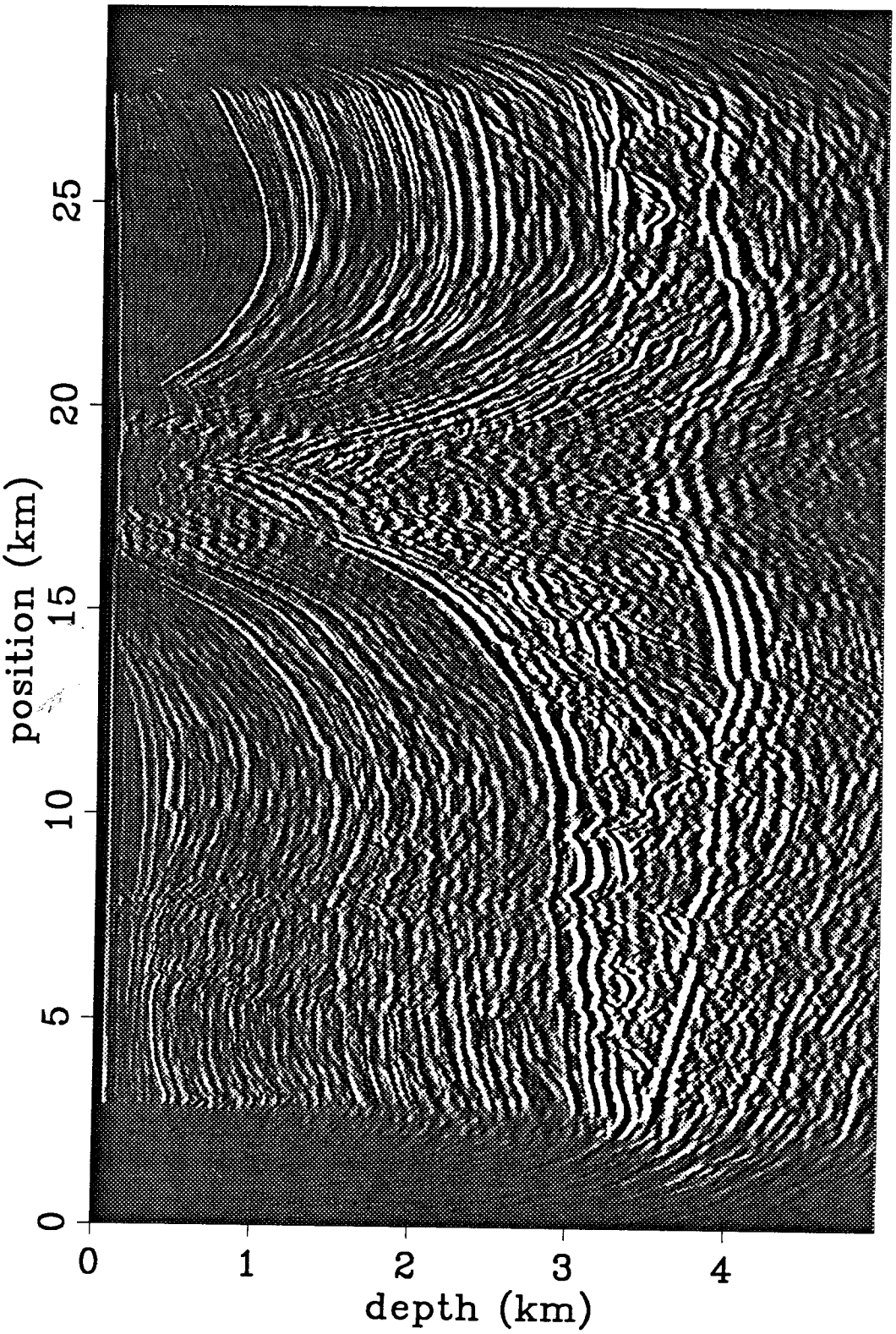

FIG. 5.5. Stacked section after prestack depth migration with the initial interval-slowness model shown in Figure 5.4.

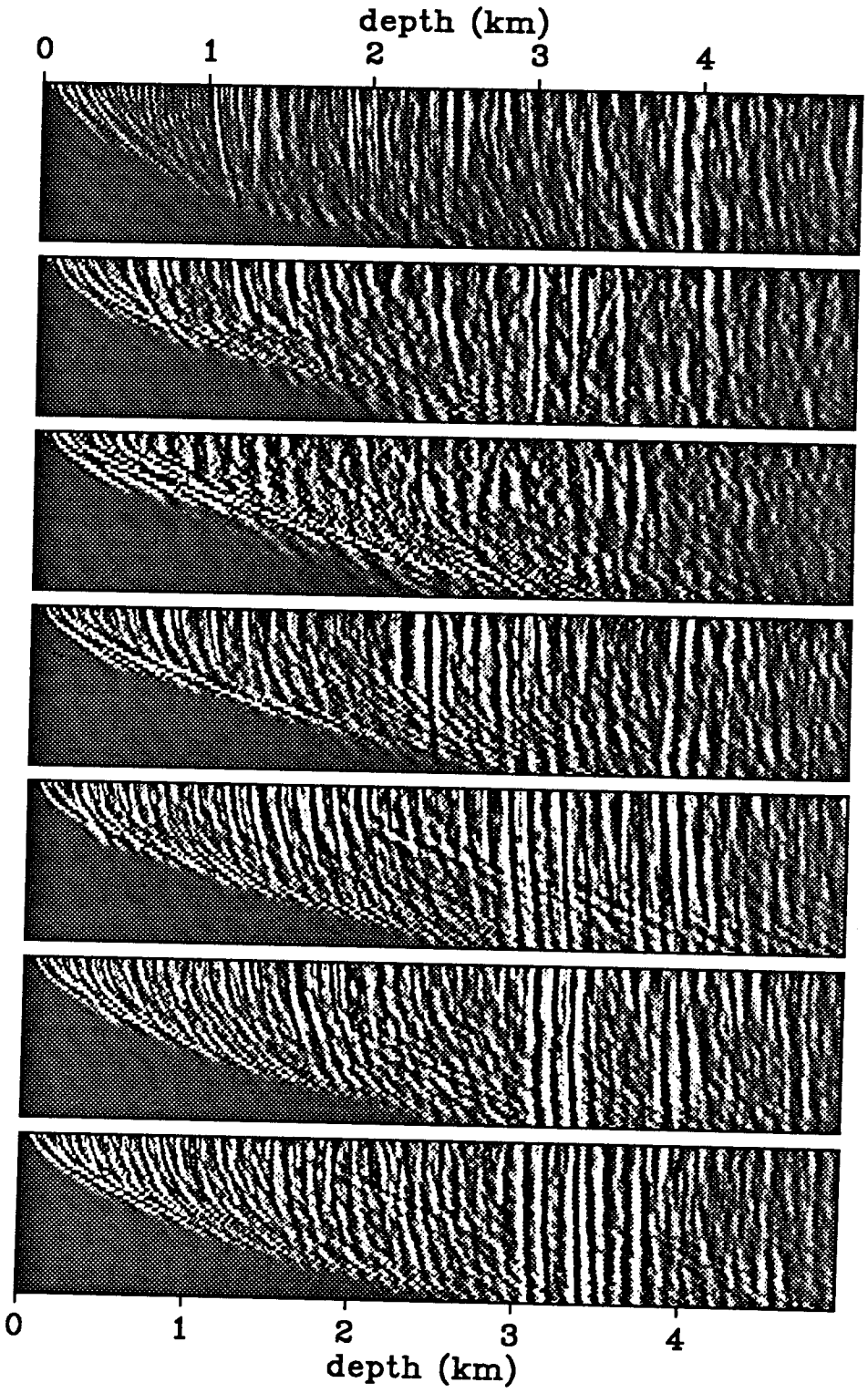

FIG. 5.6. Selected post-migration CMP gathers, taken every 3 km along the line starting at 6 km (bottom panel). The vertical axis on each panel is offset from near (top) to far (bottom). Varying amounts of residual moveout are visible indicating the initial model is incorrect. Also, the data quality is variable, especially along the bottom-of-salt reflector.

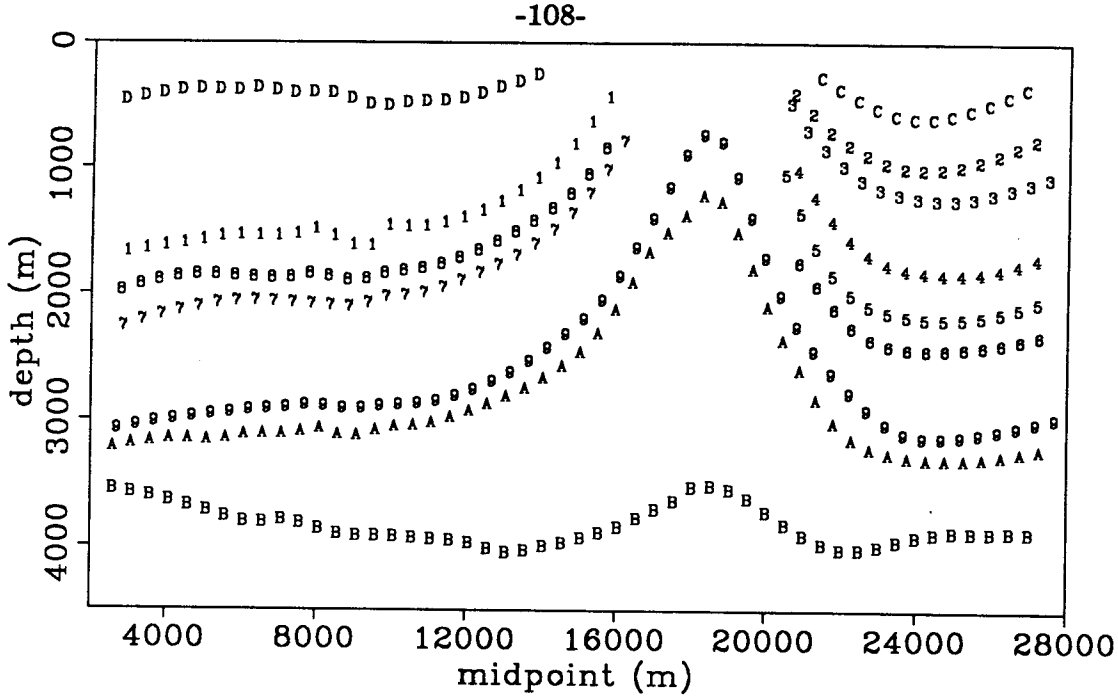

FIG. 5.7. Event positions selected for use in the tomographic inversion for a change to the interval-slowness model. Horizon residual-slowness analyses are shown in the next figure for some of the events.

The data quality of the migrated constant-offset sections varies depending on whether one looks at the shallow sediments, the top of salt, or the bottom of salt. Unfortunately, the worst data quality is where the velocity information is likely to vary the most, near the salt dome (the fifth gather up from the bottom in Figure 5.6). The bottom-of-salt reflector is difficult to see at about 3.5 km depth, and it is not coherent in offset. Variable data quality like that observed here is one of the reasons to use semblance as an objective function rather than picking event depths or even semblance peaks. The width of the semblance function in γ weights well determined velocity information more strongly than poorly determined velocity information.

To avoid the shallow multiples and primarily to decrease the cost of computing the operator of Chapter 3, I used an interactive event picking program (Van Trier, 1990) to select several events on the stacked image to use for further velocity analysis. Figure 5.7 shows the picked events; different numbers or letters refer to different events.

To quantify the errors in the migrated images and hence in the initial model, I applied residual NMO+DMO to the migrated constant-offset sections for a range of residual slownesses and built a residual-slowness analysis cube. The intensity plot of Figure 5.8 shows horizon residual-slowness analyses for some of the numbered events in Figure 5.7.

The positions of the peaks of the semblance (shown in lighter shades) quantify the moveout of each reflector in terms of residual slowness. The next step in the velocity-analysis algorithm of Chapter 4 is to compute $\mathbf{G}$ and solve the inner optimization problem by conjugate-gradients and try to explain the observed residual slownesses. Thus, the objective function for the inner loop consists of the semblances versus γ and reflector position for all events in Figure 5.7.

I ran the conjugate gradient iterations (inner-loop iterations) to convergence, i.e., when $\nabla_{\mathbf{w}} Q \approx 0$. The dark curves overlying each panel in Figure 5.8 show γ predicted by the update to the interval-slowness model Δw. With a few exceptions where the velocity information is sparse or not coherent, the conjugate-gradient optimization was able to find and explain the peaks of semblance. I used a smoothness constraint on the interval-slowness model, so the model should be smooth where it is not constrained by the velocity information from the reflectors. The dark line leaving the panel on the second row is due to this smoothness constraint. Since there was little velocity information through the center of the salt dome, the high velocities initially there were smoothed out and decreased to make the model smoother.

Figure 5.9 shows Δw obtained with the conjugate-gradient optimization and the new slowness model obtained by adding Δw to the original interval-slowness model. To find out if the new slowness model reduces the amount of residual moveout and gives a better image, remigrate the data. Figure 5.10 shows the depth-migrated and stacked section obtained using the new interval-slowness model of Figure 5.9. The positions of the sediments above the left flank of the salt dome have been altered; the image of the bottom-of-salt reflector has also been altered. One area along the bottom-of-salt reflector, corresponding to the region of low γ in Figure 5.7 reflector B, has been deepened relative to the neighboring parts of the bottom of salt. Strangely, the part of the bottom-of-salt reflector where the reflected waves must travel through the most salt is pulled up from the surrounding parts of the reflector. It is not clear yet if this is true structure or an artifact.

Figure 5.11 shows the events selected from the stacked section to be used for another outer iteration of velocity analysis. To reduce the cost of performing prestack depth migration, I partially stacked the input constant-offset sections before applying prestack depth migration with the new model. Partial stacking reduced the number of viable offsets in the shallow part of the data, so I omitted the shallowest events seen in Figure 5.7 from further velocity analysis.

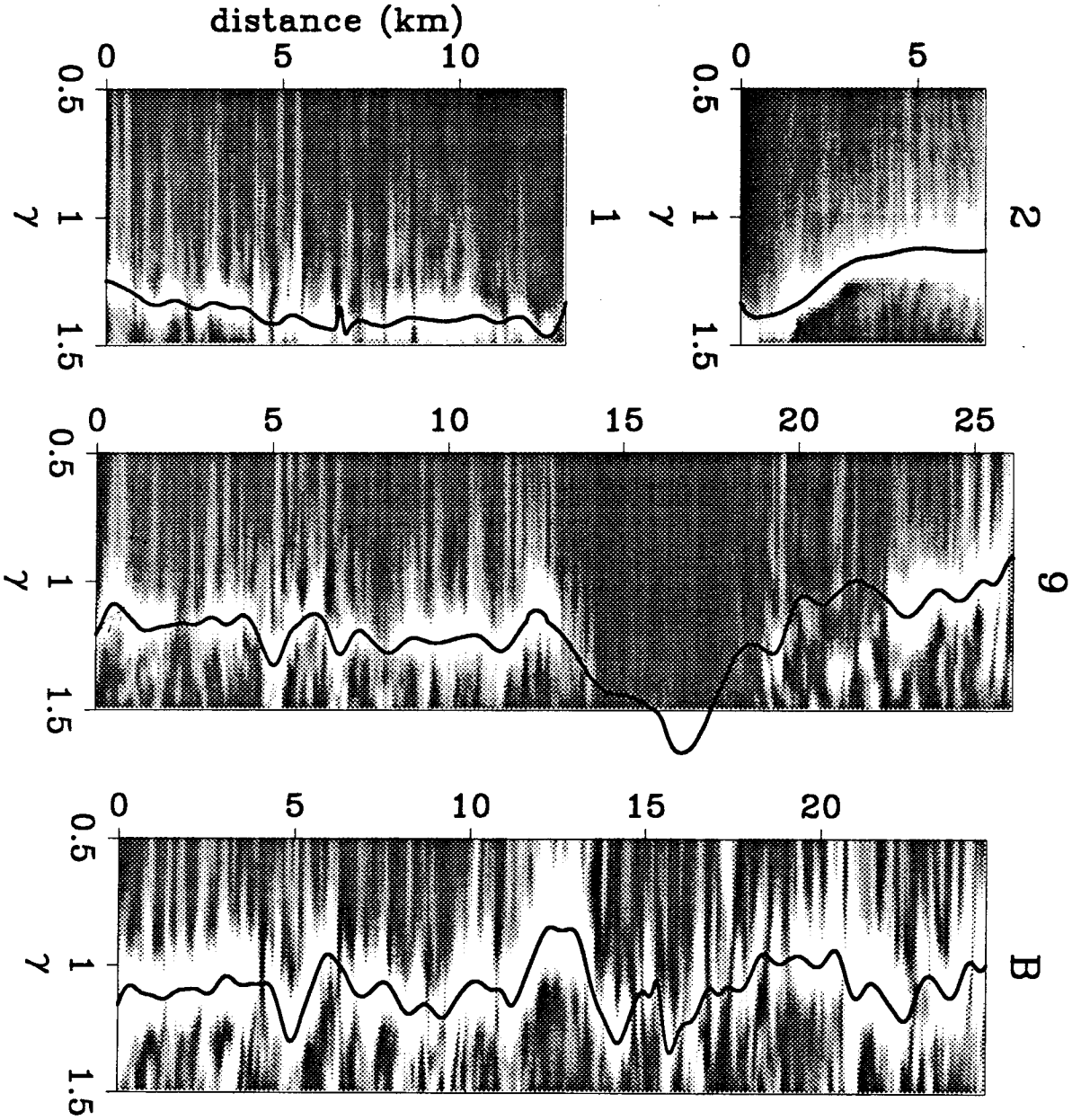

FIG. 5.8. Horizon residual-slowness analyses for some of the events in Figure 5.7. The event number in Figure 5.7 corresponds to the number on the right of each panel. The overlying dark curves show the values of γ predicted by the change to the interval-slowness model after solving the inner optimization problem.

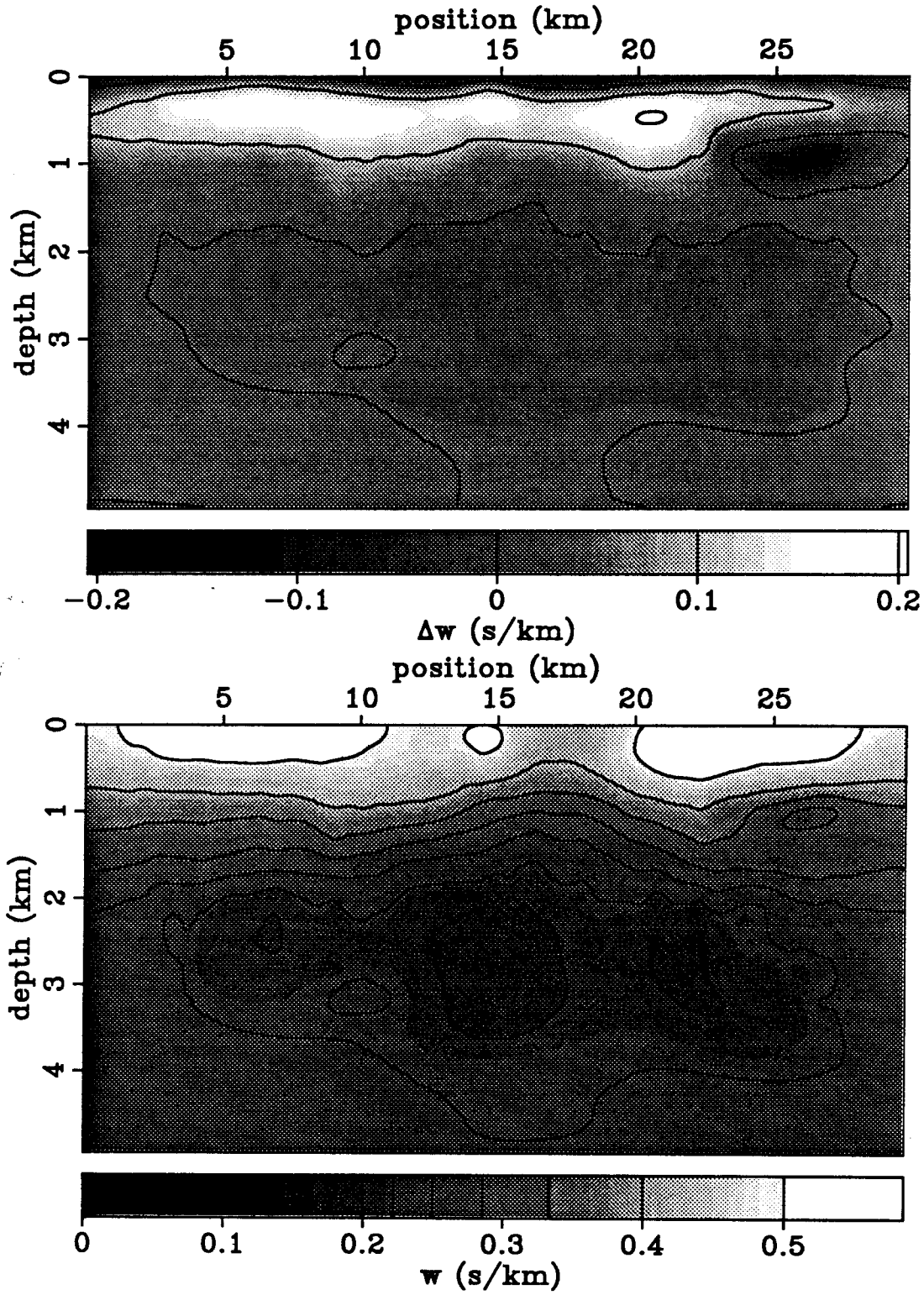

FIG. 5.9. The top plot shows the change to the interval-slowness model obtained by solving the inner optimization problem. The bottom plot shows the new interval-slowness model.

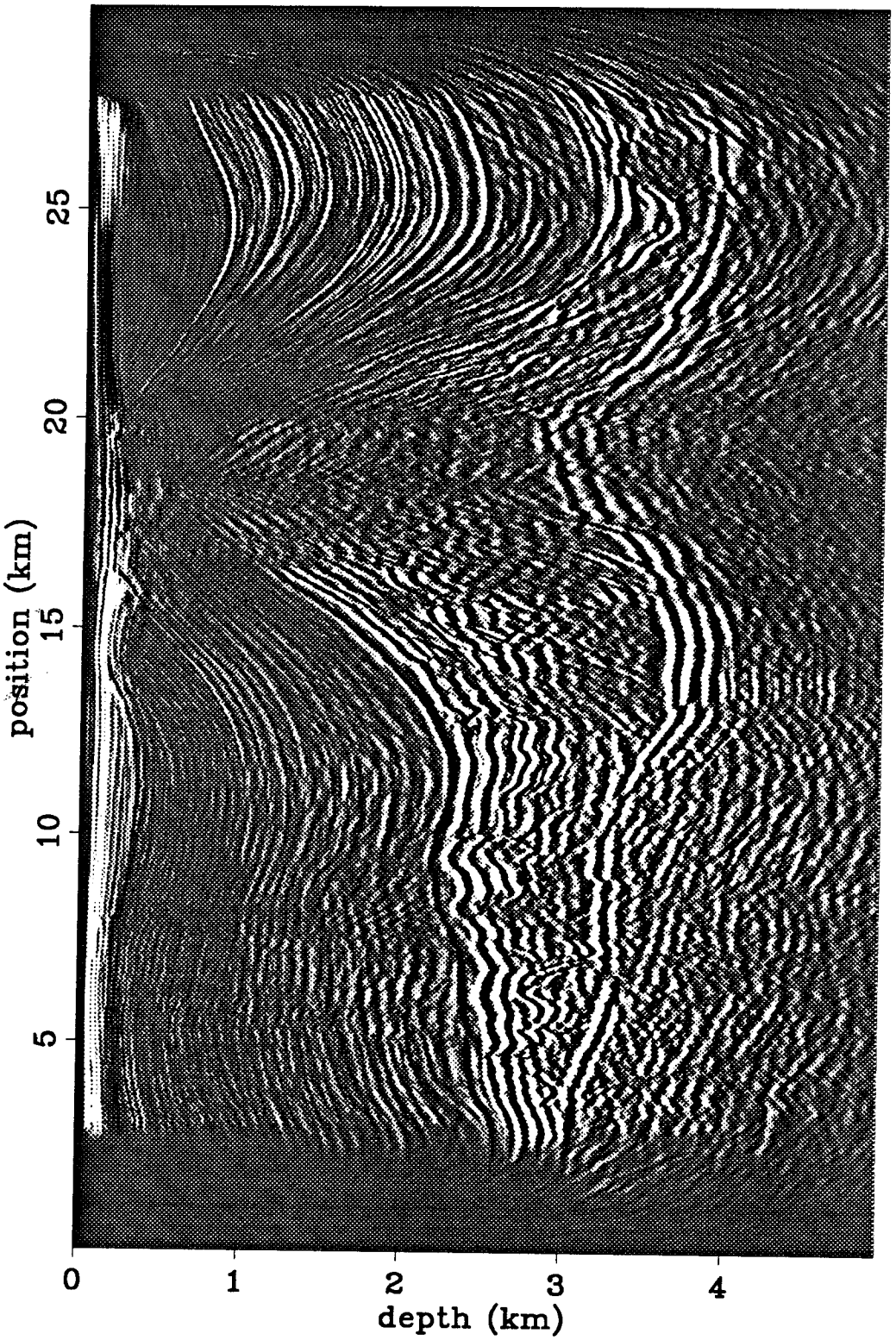

FIG. 5.10. Stacked image after applying prestack depth migration to the North Sea data set with the interval-slowness model after one iteration of velocity analysis.

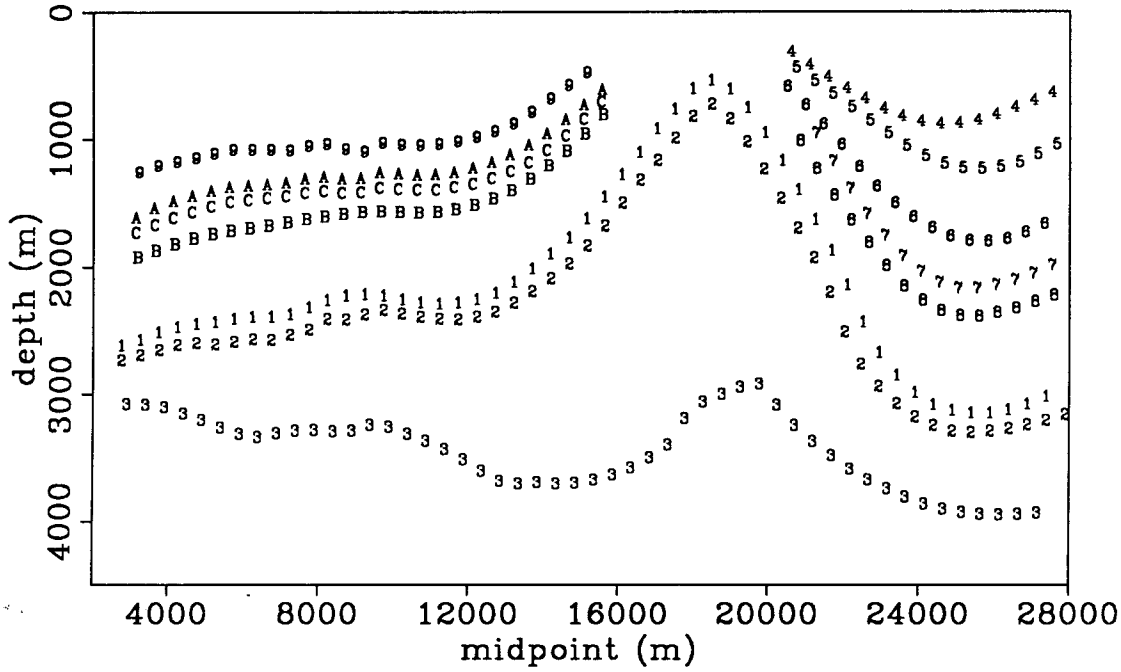

FIG. 5.11. Events selected for horizon residual-slowness analysis from the migrated and stacked section shown in Figure 5.10.

To quantify remaining residual moveout, perform residual-slowness analysis on the new migrated constant-offset sections. The intensity plot of Figure 5.12 shows horizon residual-slowness analyses for several of the reflectors in Figure 5.11. Again, the reflector corresponding to each semblance panel is labeled in Figure 5.11 with the number at the right of the panel. In general, the semblance peaks are closer to the desired $\gamma = 1$ line, but errors still exist in the interval-slowness model because the peaks are not exactly at $\gamma = 1$. Referring back to the residual-slowness analysis of Figure 5.8, notice that the correction to the model made by the first outer iteration was an over-correction. Many of the events that had semblance peaks at $\gamma > 1$ now have peaks at $\gamma < 1$. The over-correction is caused by the nonlinearity of the problem; $\mathbf{G}$ cannot correctly model all the effects of a large perturbation to the interval-slowness model.

I ran one more outer iteration of velocity analysis, again solving the inner optimization problem to completion. The dark curves overlying the semblance values in Figure 5.12 show the values of γ predicted by the change to the interval-slowness model found during

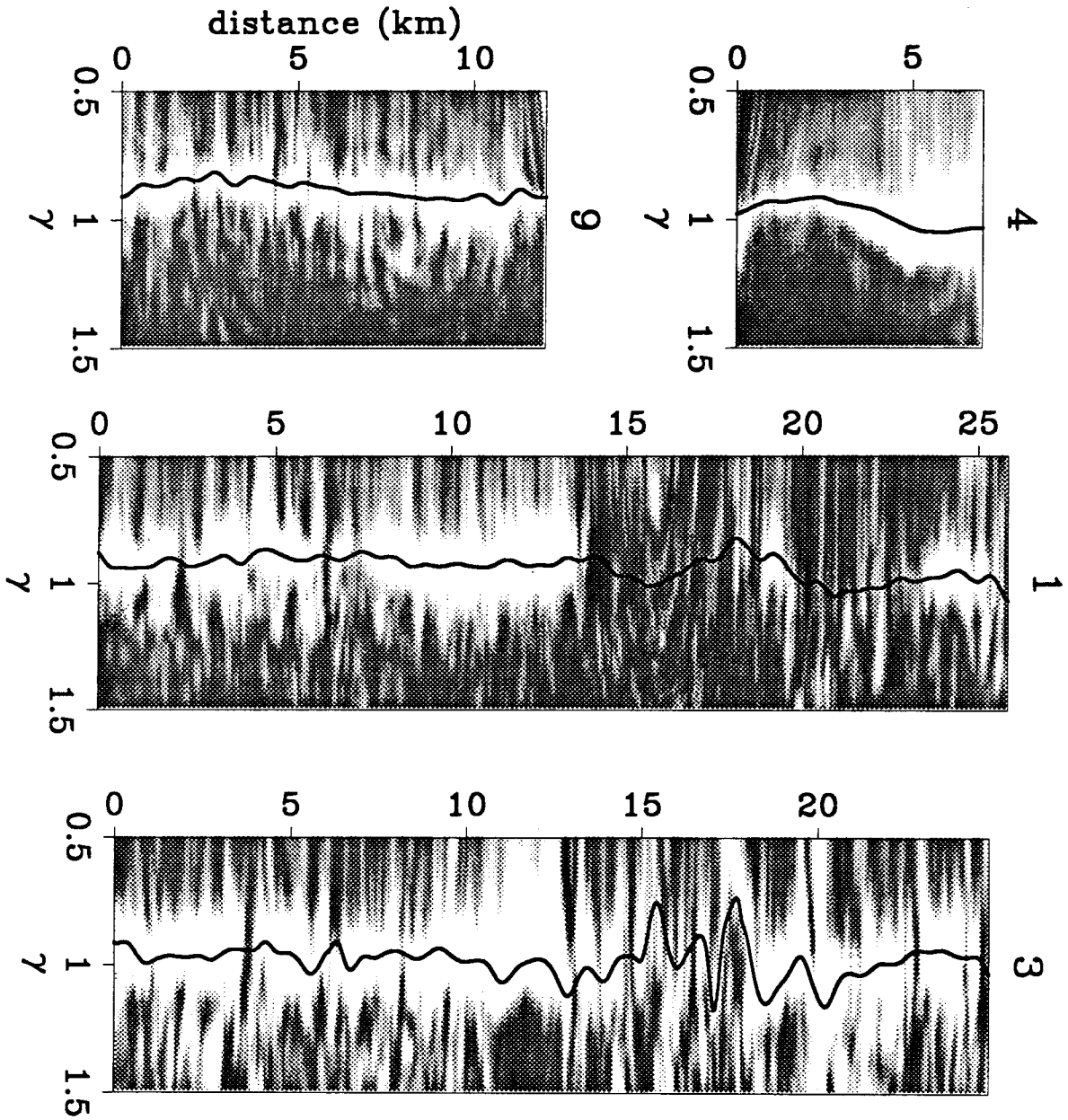

FIG. 5.12. Horizon residual-slowness analyses for 4 reflectors in the migrated section of Figure 5.10. The number tells the horizon plotted in Figure 5.11 corresponding to the semblance panel.

the second iteration. As before, the inner optimization problem was able to find and explain the positions of the semblance peaks. Figure 5.13 shows the final interval-slowness model and the cumulative change in interval slowness from the initial model. The smoothness constraint smoothed the model where the velocity information was sparse, but lateral variation still exists within the salt dome where it is unlikely to be real. Figure 5.14 shows the final stacked section obtained by migrating the data set before stack with the interval-slowness model of Figure 5.13. The image of the bottom of salt has substantially changed from the initial migration. Figure 5.15 and 5.16 show selected events and their horizon residual-slowness analyses. Now the semblance peaks are much closer to the line $\gamma = 1$; this means that the final model produces migrated constant-offset sections that have little or no residual moveout over offset. Figure 5.17 shows a section of the final migrated image around the salt-dome plotted with no vertical exaggeration.

As we saw in Chapter 4, the final interval-slowness model accounts for the moveout in the data; but the structural image may be inaccurate. The long-wavelength structure on the bottom-of-salt reflector is suspect because of the null space of $\mathbf{G}_\gamma$. However, there are indications that some of the structure is real. In Figures 5.14 and 5.17, the bottom of salt appears to be broken by faults; the best example is the fault near midpoint 17.5 km. Although initial interpretation of the CMP stacked section in Chapter 1 might indicate a horizontal bottom of salt (after removing the pull-up), the final image suggests horst and graben fault-block structure. Movement along the faults that raised the horst might have contributed to salt movement (Bally, 1983). The faults in the sediments of the left part of the line suggest that the salt squirted out from beneath the sediments and rose above the horst. These listric faults on the left side of the dome could also have been caused by regional stress; combined with the block faulting below the salt, the regional stress might have caused a weakened zone that allowed the unstable salt to swell. Thinning of the sediments onto and above the dome indicate that salt movement was rapid during more recent times when the shallow sediments were deposited.

Although the amount of structure or the extent of vertical relief is uncertain, I find it unlikely that the bottom of salt is horizontal. Furthermore, an interval-slowness model (Figure 5.4) that produced an nearly horizontal bottom of salt does not agree with the traveltimes in the data.

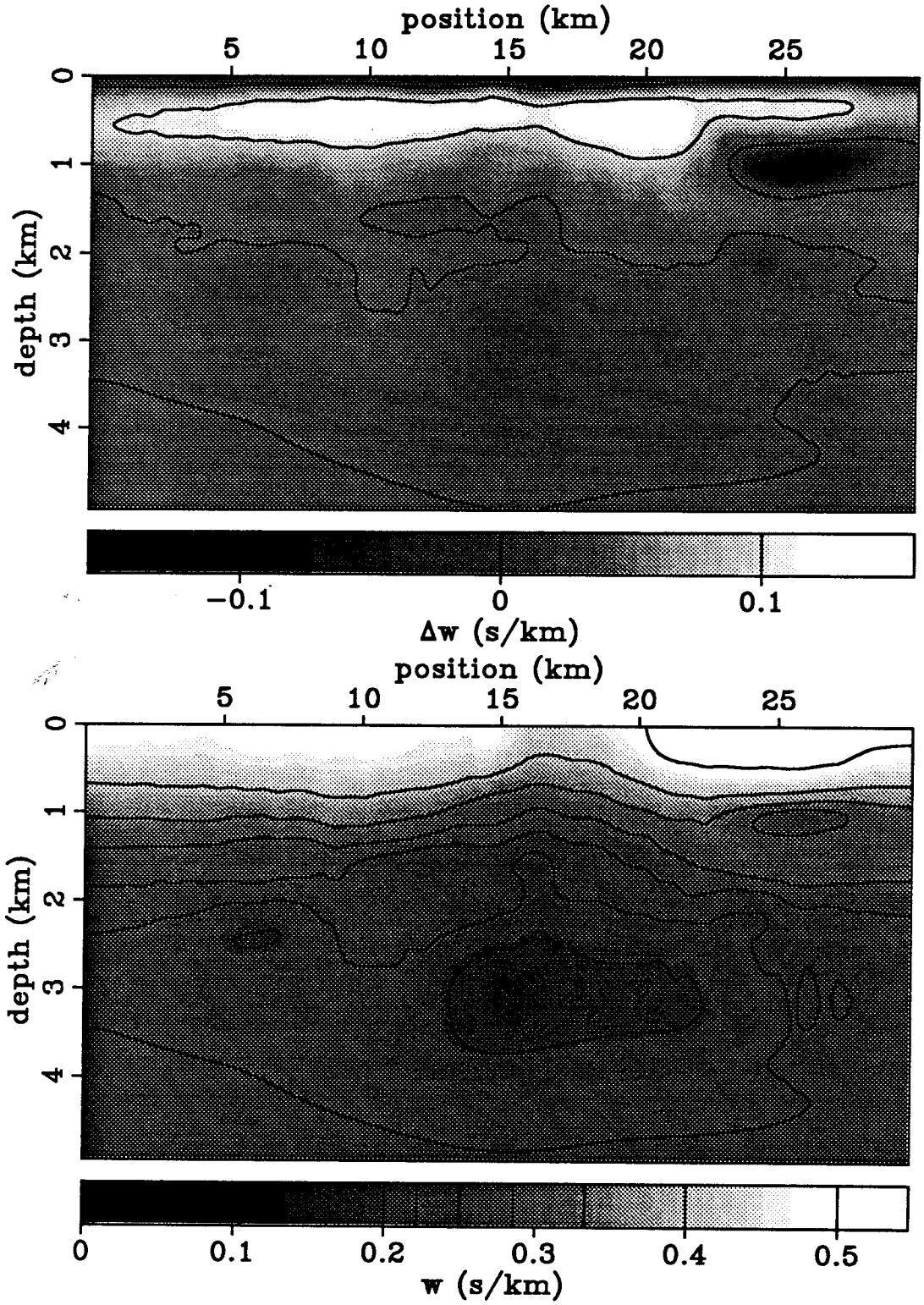

FIG. 5.13. The top plot shows the cumulative change to the interval-slowness model after two iterations. The bottom plot shows the final interval-slowness model.

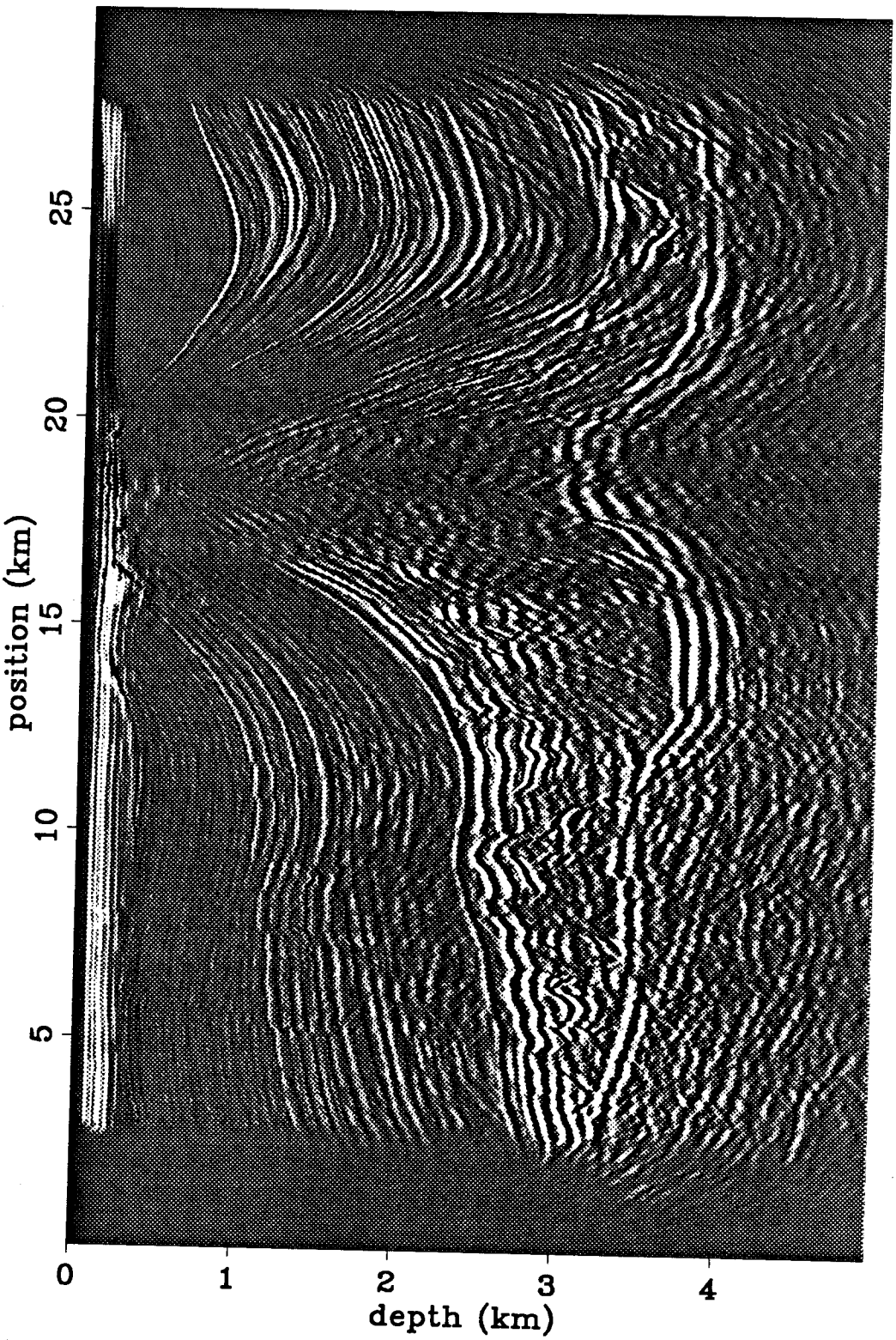

FIG. 5.14. Stacked image after applying prestack depth migration to the North Sea data set using the final interval-slowness model (Figure 5.13).

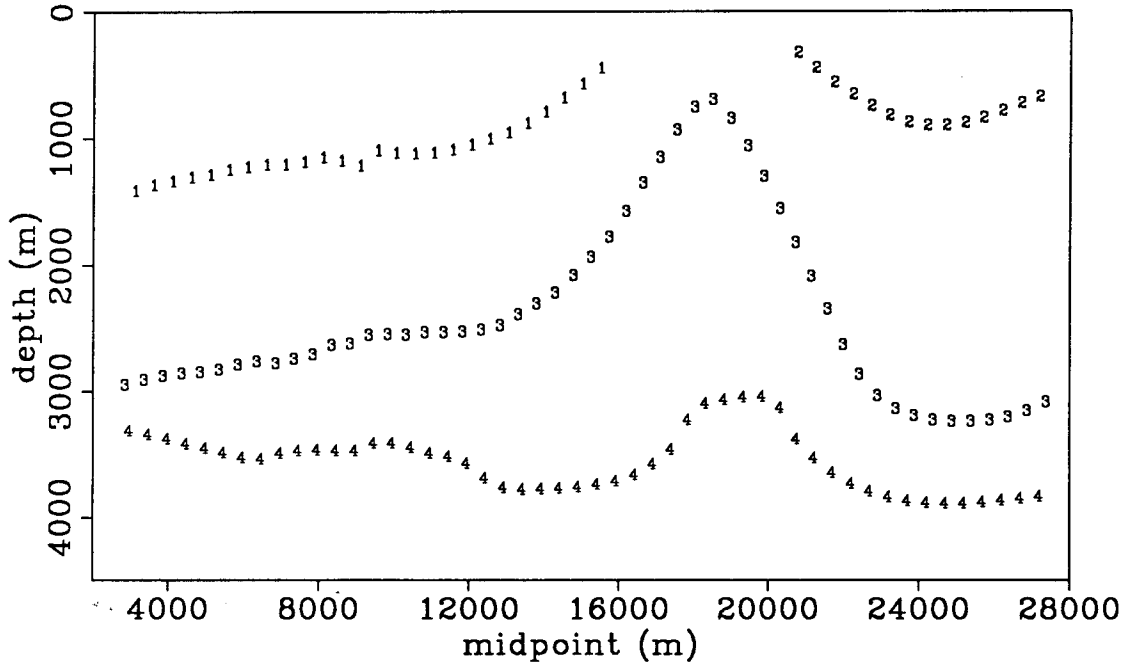

FIG. 5.15. Events selected for horizon residual-slowness analysis after the final prestack depth migration.

5.3 Discussion and conclusions

In both the synthetic example of Chapter 4 and the field-data example above, multiple outer iterations were required to find an interval-slowness model that produced migrated images with no residual moveout. The primary reason for this: the operator of Chapter 3 is only approximate and does not accurately predict the effect of a large perturbation to the interval-slowness model. In both the synthetic example and the field-data example, large changes to the interval-slowness model were required to go from the initial model to the final model. The need for multiple outer iterations is a weakness of the velocity-analysis method presented here. Prestack depth migration is expensive, so one prefers to do it only once, or if the initial migration is wrong, to be able to correct it in one iteration. Unfortunately, a theory like the one of Chapter 3 that fully accounts for the effect of an arbitrary change to the interval-slowness model would be difficult or impossible to derive. Since they are necessary anyway, the remigrations required in the outer iterations

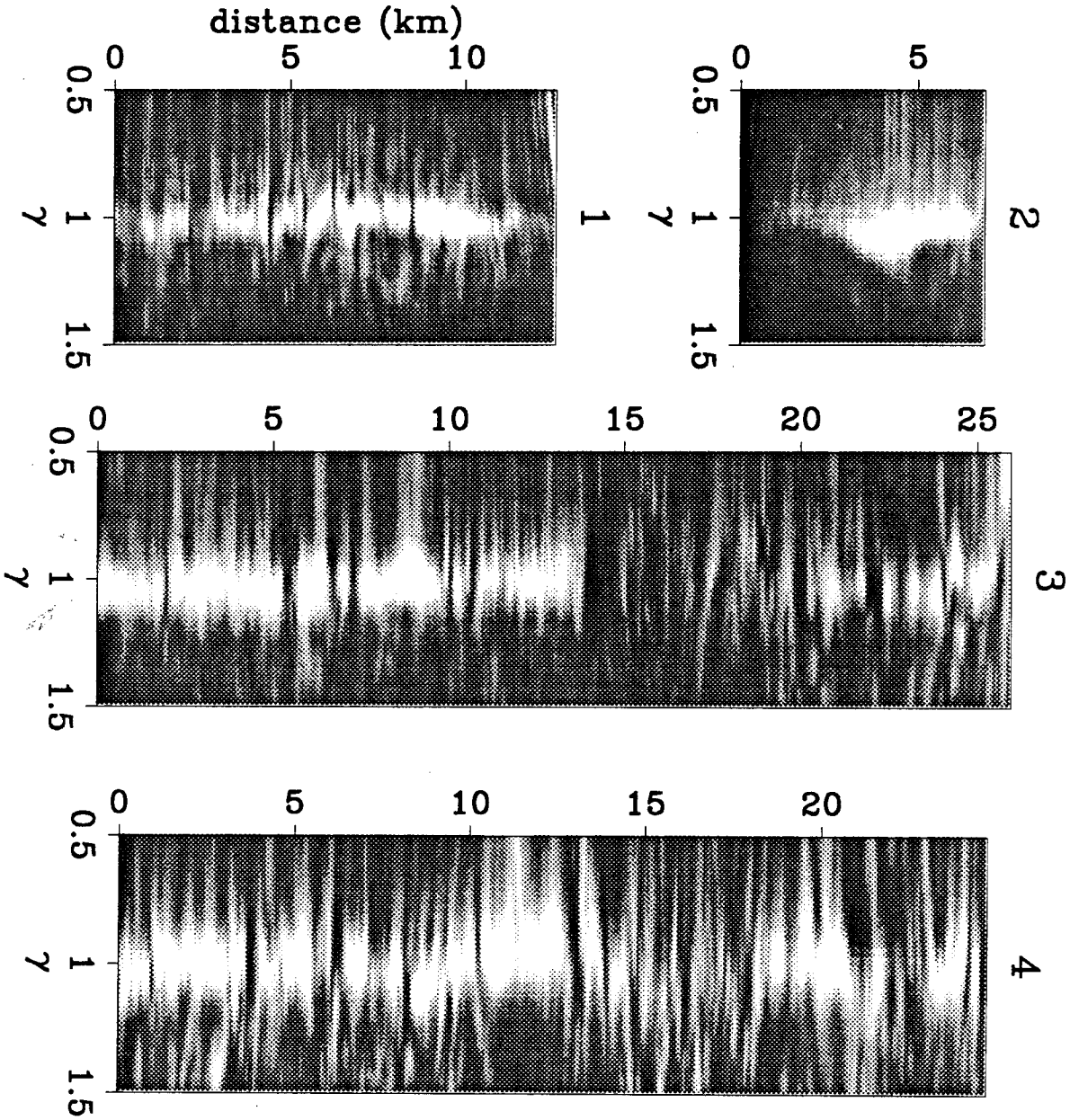

FIG. 5.16. Horizon residual-slowness analyses for the four events shown in Figure 5.15. Most semblance peaks are now within 2-5% of $\gamma = 1$.

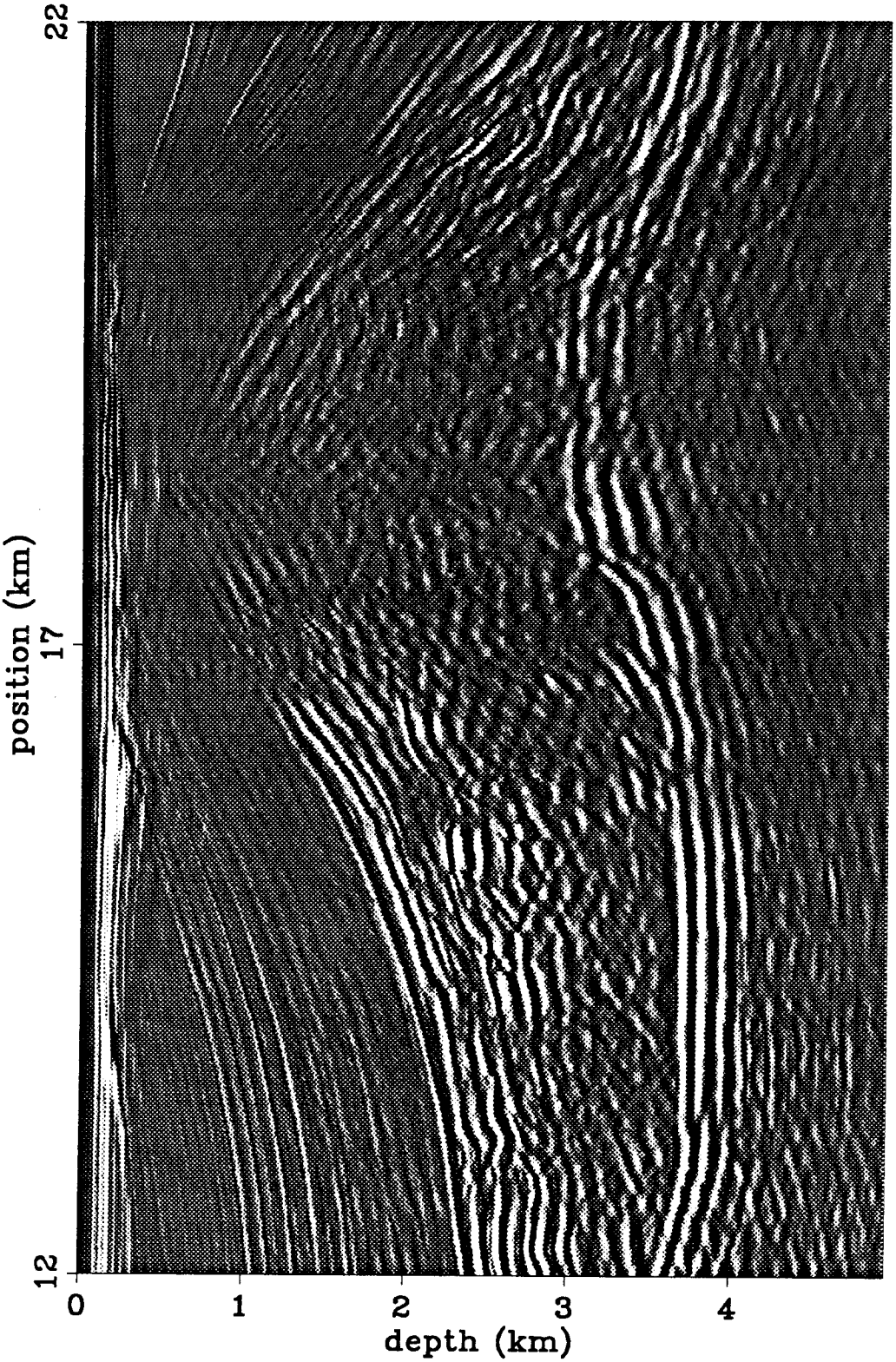

FIG. 5.17. Central part of the stacked image obtained with prestack depth migration using the final interval-slowness model (plotted with no vertical exaggeration). A fault explains some of the relief seen on the bottom-of-salt reflector.

provide a sanity check. One can see how the migrated image changes as the interval slowness changes rather than only getting one final image. This presents the opportunity to steer the inversion by picking more or fewer events or just different events for each iteration. Also, different amounts of smoothness constraints can be applied for different iterations. The synthetic example showed that it is best to begin trying to estimate a smooth model and relax the smoothness constraints only after the reflectors are nearly correctly positioned. Then it is possible to extract information about higher-wavenumbers of the slowness model if the data quality will allow.

Although semblance is a more robust objective function than a least-squares criterion for picked moveout or traveltimes, velocity analysis based on semblance is still sensitive to data quality. In the real-data example above, obtaining reliable residual-slowness analyses for the bottom-of-salt reflector was difficult due to poor data quality in some areas. Inversion of $\mathbf{G}$ uses the lateral variation in the measured residual slownesses, so the lack of coherent velocity information on top of and below the salt dome hampers the ability of the algorithm to derive an interval-slowness model there. The smoothness constraint helped, but could not determine the interval slowness by itself.

A velocity-analysis method based on picking might appear to give a good answer because some model that fits the picks can be found, but the reliability of the model is in doubt because the picks themselves would be unreliable. The danger present when "inventing" data, is inventing the wrong data. Using semblance as an objective function takes the data quality into account. Although picked traveltime tomography or even picked event tomography (Van Trier, 1990) might seem easier, using semblance as an objective function is more robust, and doesn't invent velocity information when none in present in the data. Sometimes the information in the data is inadequate or noisy, and a trained interpreter might be able to invent picks that will migrate the data and provide a better image than that obtained by a more automatic method simply because the invented data were fortuitously correct.

The synthetic example showed that when there aren't enough reflectors to provide velocity information, the null space of the $\mathbf{G}_\gamma$ operator affects the estimation of interval slowness. Two different interval-slowness models can produce the same residual-slowness analysis, but not the same structure. The long-wavelength structure on the deeper reflector in Figure 4.6 is of roughly the same wavelength as that predicted by the zero of the spectrum of the $\mathbf{G}_\gamma$ operator for anomalies near the surface. The $\mathbf{G}_\tau$ operator has a

different null space, so although the migrated image had little or no residual moveout, there were differences between the migrated position of the reflector and its true position.

For the synthetic, it is possible to "cheat," and invert the $\mathbf{G}_\tau$ operator and get better structural results. Unfortunately, with real data we don't often know the positions of reflectors so we can't invert the $\mathbf{G}_\tau$ operator to constrain the results. In the North Sea example we see evidence of the null space of $\mathbf{G}_\gamma$; the bottom-of-salt reflector has long-wavelength structure as well. Some of the structure may be real, especially where there are sharp changes in slope; but structure with a wavelength of about 10 km is suspect since there is little information constraining the interval velocities above the salt dome. Biondi's (1990) velocity-analysis method addresses this problem by fitting the data over only part of the cable, instead of over the whole cable as I have done here. This increases the number of independent parameters and reduces the filtering effects of stacking and thus reduces the null space. The method of this thesis could be modified to use multiple residual-slowness analyses obtained by stacking over smaller segments of the cable to decrease the null space. Although using more parameters reduces the null space, it also reduces data reliability; there is a trade-off. For the North Sea data set, there is a problem with both the null space and data quality. I don't think that meaningful residual-slowness analyses could be made from smaller segments of the cable along most of the bottom-of-salt reflector, so the data reliability issue is more important, and stacking over the whole cable is necessary for this data set.

At the outset, I designed the velocity-estimation method of this thesis to be automatic. The method is successful in producing migrated constant-offset sections with no residual moveout. Unfortunately, unless the quality of velocity information is high and the reflectors are sufficiently dense, a model that produces no residual moveout is non-unique. Since the inversion, as I have posed it, has no way of knowing what structure is correct, structural artifacts can creep into the image. The role of an interpreter during interval-velocity estimation is to provide the extra knowledge that can constrain the interval-slowness model when the data does not. In this thesis, I have only used simple smoothness constraints and reflector selection to fulfill this role. Making interval-velocity estimation a routine process in areas of complex structure and lateral velocity variation will require a clever integration of the automatic part of velocity analysis as well as the interpretive part.